Atmos. Chem. Phys. Discuss., 11, 9673–9703, 2011
www.atmos-chem-phys-discuss.net/11/9673/2011/
doi:10.5194/acpd-11-9673-2011

Atmospheric Chemistry and Physics Discussions

Resolving both entrainment-mixing and number of activated CCN in deep convective clouds

E. Freud[1], **D. Rosenfeld**[1], **D. Axisa**[2], **and J. R. Kulkarni**[3]

[1]The Hebrew University of Jerusalem, Jerusalem, Israel
[2]National Center for Atmospheric Research, Boulder, CO, USA
[3]Institute of Tropical Meteorology, Pune, India

Received: 24 February 2011 – Accepted: 15 March 2011 – Published: 22 March 2011

Correspondence to: E. Freud (eyal.freud@mail.huji.ac.il)

Published by Copernicus Publications on behalf of the European Geosciences Union.

Abstract

The number concentration of activated CCN (N_a) is the most fundamental microphysical property of a convective cloud. It determines the rate of droplet growth with cloud depth and conversion into precipitation-sized particles and affects the radiative properties of the clouds. However, measuring N_a is not always possible, even in the cores of the convective clouds, because entrainment of sub-saturated ambient air deeper into the cloud lowers the concentrations by dilution and may cause partial or total droplet evaporation, depending on whether the mixing is homogeneous or extreme inhomogeneous, respectively.

Here we describe a methodology to derive N_a based on the rate of cloud droplet effective radius (R_e) growth with cloud depth and with respect to the cloud mixing with the entrained ambient air. We use the slope of the tight linear relationship between the adiabatic water and R_e^3 to derive an upper limit for N_a assuming extreme inhomogeneous mixing. Then we tune N_a down to find the theoretical relative humidity that the entrained ambient air would have for each horizontal cloud penetration, in case of homogeneous mixing. This allows us to evaluate both the entrainment and mixing process in the vertical dimension in addition to getting a better estimation for N_a.

We found that the derived N_a from the entire profile data is highly correlated with the independent CCN measurements from below cloud base. Moreover, it was found that mixing of sub-saturated ambient air into the cloud is inclined towards the extreme inhomogeneous limit, i.e. that the time scale of droplet evaporation is significantly smaller than that for turbulent mixing. This means that ambient air that entrains the cloud is pre-moistened by total evaporation of cloud droplets before it mixes deeper into the clouds where it can hardly change the droplet size distribution, hence R_e remains close to its adiabatic value at any given cloud depth. However, the tendency towards the extreme inhomogeneous mixing appeared to slightly decrease with altitude, possibly due to enhanced turbulence and larger cloud drops aloft.

ACPD
11, 9673–9703, 2011

Quantifying these effects, based on more examples from other projects and high resolution cloud models is essential for improving our understanding of the interactions between the cloud and its environment. These interactions may play an important role in cloud dynamics and microphysics, by affecting cloud depth and droplet size spectra, for example, and may therefore influence the cloud precipitation formation processes.

1 Introduction

Clouds are responsible for two thirds of the planetary albedo and hence play a dominant role in determining the Earth energy budget and the global temperature. Aerosols affect cloud albedo by nucleating larger number of smaller droplets that enhance the light scattering for a given amount of cloud water (Twomey, 1974). According to the IPCC (2007) report, the uncertainty in the aerosol cloud albedo effect, particularly in the anthropogenic aerosol component, dominates the uncertainty of the climate radiative forcing. Aerosols can also alter the cloud coverage and lifetime of both cooling (Albrecht, 1989) and warming (Koren et al., 2010), and significantly affect the precipitation processes and hence the redistribution of heat and energy in the atmosphere (Rosenfeld et al., 2008a). This occurs through the aerosol impacts on precipitation forming processes and the following modification of cloud dynamics. These processes are at least as important and even less understood than the albedo effect which was highlighted as the main source of uncertainty (IPCC, 2007).

Aerosols and clouds are microphysically related through the number of the activated aerosols that serve as cloud condensation nuclei (CCN) and produce cloud droplets. This depends on the sizes, concentrations and chemical properties of the aerosols as well as on the super-saturation that they were exposed to. As long as the droplet concentrations and their surface areas are too small to balance the super-saturation produced by the cooling of the rising saturated air, more CCN will activate into cloud droplets. Stronger updrafts will result in higher droplet concentrations. Direct measurements of CCN activity cannot be made by remote sensing techniques, as the supersaturation needs to be controlled and adjusted. Even relating the much more common

ACPD
11, 9673–9703, 2011

retrievals of aerosol optical depths (AOD) to CCN concentrations at a given super-saturation can be problematic, because the same retrieved AOD can be the result of significantly (orders of magnitude) different CCN concentrations (Andreae, 2009).

The number of activated CCN (henceforth: N_a) into cloud droplets is the most fundamental microphysical property of a convective cloud. It determines the rate of the droplets' growth with cloud depth and in turn their conversion into precipitation-sized particles. It also affects the radiative properties of the clouds as higher concentrations will reduce the droplet sizes for a given amount of cloud water (Twomey, 1974). N_a embody not only the CCN activation spectra, but also the actual super-saturation that these CCN were exposed to. However, direct measurement of N_a is usually not possible because entrainment of sub-saturated ambient air into the cloud decreases the cloud droplet concentrations by evaporation and dilution. Even the cores of deep convective clouds, where measurements are normally avoided due to the strong vertical motions and icing hazards, are prone to entrainment. This is mainly because of their fairly small horizontal extent and the strong turbulence in and near the convective clouds. Indirect measurements of N_a by satellite and lidar retrievals were previously applied to shallow marine stratiform clouds, with the main assumption that the clouds are composed of nearly adiabatic elements (Bennartz, 2007; Brenguier et al., 2000; Schüller et al., 2003; Snider et al., 2010). These retrievals had large uncertainties and were not always validated with direct measurements. Furthermore, that methodology is not applicable to convective clouds due to a large departure from the assumption that they are close to adiabatic, and also due to the variable cloud top heights and depths at scales smaller than the typical satellite sensor resolution.

Here we introduce a methodology for deriving N_a of convective clouds, regardless of the exact knowledge of the Earth's surface radiative properties and in a wide range of aerosol and cloud droplet concentrations, and even for diluted clouds. This methodology, presented in Sect. 3, is based on in-situ measurements of the cloud droplet spectra at different levels in clouds. But first we discuss the entrainment-mixing process of sub-saturated ambient air into the cloud in Sect. 2.

ACPD
11, 9673–9703, 2011

2 Entrainment-mixing processes

Typically, as soon as a convective cloud is formed in a super-saturated rising bubble of air, it continues to grow upwards into a layer of sub-saturated air. As long as the cloud is not precipitating and without significant dilution by entrained air, its liquid water content (LWC) is expected to be close to the adiabatic water content (LWC_a). Nearly adiabatic values of LWC are often measured in St and Sc clouds because of their relatively wide extent so that much of their cloud volume does not come into contact with the surrounding sub-saturated air. Convective clouds, however, have a much smaller horizontal dimension and are more turbulent, so that the entrained sub-saturated air from the surroundings of the clouds has a high chance of quickly penetrating deeper into the cloud and reaching its adiabatic core while lowering LWC by dilution. The cloud droplets that are exposed to that sub-saturated air will partially or completely evaporate and increase the water vapor partial pressure in the entrained air, until it is saturated. The fate of the droplets is determined by the mixing proportions of the cloudy and ambient air, its relative humidity (RH) and the sizes and concentrations of the droplets. Without mixing, precipitation, secondary droplet nucleation and droplet coalescence, the mean droplet radius (by volume), henceforth R_v, is expected to be equal to the mean droplet radius in an adiabatic parcel (R_{v_a}), which only depends on N_a and LWC_a (Eq. 1). Again, model and airborne studies reveal that in Sc clouds, R_v and R_{v_a} are quite similar, except for close to the cloud edges, and especially near the top of the cloud where most mixing occurs (e.g. Pawlowska et al., 2000). How exactly mixing and entrainment affect the droplet size distribution and R_v is an issue that has been studied for more than three decades and there is still no satisfying answer, specifically in convective clouds. This is because mixing starts with eddies with a length scale of tens or hundreds of meters that gradually break into smaller filaments down to the Kolmogorov microscale (~1 mm in normal atmospheric conditions), where variations in temperature and water vapor fields are homogenized by molecular diffusion. Such scales cannot be explicitly resolved by today's cloud models and standard airborne cloud microphysics instrumentation (Baker et al., 1984; Brenguier, 1993; Lehmann et al., 2009).

ACPD
11, 9673–9703, 2011

Until the late 1970s the research of the entrainment-mixing process was based on the idea that the cloud droplets at any given level are equally exposed to the entrained sub-saturated air, regardless if their specific location in the cloud, and as a result evaporate partially or completely together – what was later described as homogeneous mixing by Baker et al. (1980). In a laboratory study, Latham and Reed (1977) found that concentrations of small droplets become very inhomogeneous after admixture with sub-saturated air, because some of the droplets totally evaporate while others remain unchanged. This finding helped explain some of the discrepancies between earlier calculations and modeling results, and observations in clouds. In their published studies, Baker et al. (1980) and Blyth et al. (1980) set the grounds for the current research on the effect of mixing and entrainment on cloud droplet spectra. They defined the range of the mixing effect on cloud droplet spectra based on the time scales of droplet evaporation (τ_{evap}) vs. turbulent mixing (τ_{mix}). In the case that $\tau_{evap} \ll \tau_{mix}$ the droplets that border the entrained air bubble or filament will quickly evaporate until the entrained air becomes saturated, so further mixing will only dilute the rest of the cloud droplets and will leave the shape of the droplet spectra unchanged. This is referred to as the extreme inhomogeneous case. The other extreme is the homogeneous mixing. It fulfills the condition: $\tau_{evap} \gg \tau_{mix}$. That means that the sub-saturated air will be first fully mixed in the cloud volume, so all droplets will be exposed to the same sub-saturation, and then will partly evaporate until the air becomes saturated again. This will cause the droplet size spectra to shift towards the smaller sizes but the number of droplets will remain the same. In reality though, the ratio between τ_{mix} and τ_{evap}, also called the Damköhler ratio (Dimotakis, 2005), is typically not much smaller or larger than unity. It depends on the mixing scales, turbulence, the ambient RH, the droplets' sizes and concentrations etc. (Lehmann et al., 2009).

Figure 1 shows an example of the theoretical relationship between the mean droplet radius (R_v) and the adiabatic fraction (AF), which is the ratio between LWC and LWC_a, for extreme inhomogeneous and fully homogeneous mixing scenarios. We use common values for the parameters that affect this relationship to get typical values of

ACPD
11, 9673–9703, 2011

R_V. This figure resembles the mixing diagram shown in Burnet and Brenguier (2007), but here we plot AF on the abscissa rather than the normalized number of droplets, because it represents better the amount of entrained air that the adiabatic parcel has been mixed with. How much the droplets will reduce in size in relation to R_{V_a} when exposed to sub-saturated air is determined by the initial water vapor content of the entrained air: the drier it is the smaller the droplets will become upon mixing and saturation of the entrained air, until their mass is not sufficient to saturate the mixed air and they completely evaporate. Mixing with air that is already saturated, or in case of extreme inhomogeneous mixing, R_V will be equal to R_{V_a} for all adiabatic fractions. Figure 1 clearly shows that the R_V vs. AF curve strongly depends on the RH of the entrained air, but this dependence is highly non-linear: at low RH this relationship is almost independent of RH, whereas in high RH this relationship has a strong sensitivity to RH. If the RH of the entrained air is known then the deviation from the homogeneous mixing curve for that RH with respect to the extreme inhomogeneous mixing horizontal line in Fig. 1 can give an indication of the extent of the mixing inhomogeneity. For example, if the ambient RH is 30%, but the data points plotted on a mixing diagram like Fig. 1 align around the RH = 95% curve, then this would be a strong indication of mixing tendency towards the inhomogeneous limit.

Generally, it appears in the literature that the observational studies find a clear tendency towards the extreme inhomogeneous mixing (Hill and Choularton, 1985; Paluch, 1986; Bower and Choularton, 1988; Pawlowska et al., 2000; Gerber, 2006) or intermediate features between the homogeneous and inhomogeneous mixing scenarios (Jensen and Baker, 1989; Paluch and Baumgardner, 1989), although parts of it may be explained by instrumental artifacts (Burnet and Brenguier, 2007). In an earlier study of ours that analyzed many convective cloud droplet spectra in the Amazon basin (Freud et al., 2008), we also concluded that the mixing process tends towards the extreme inhomogeneous limit, as the droplet effective radii (R_e) did not show a significant dependence on the extent of droplet exposure to entrained air. Our analysis here, looks deeper into the mixing process in a quantitative way, so we are able to use

ACPD
11, 9673–9703, 2011

the deviations from the extreme inhomogeneous mixing assumptions to derive a better estimation for N_a, which is the main objective in this study.

3 Methods

The number of activated CCN, N_a, which we aim to derive, is a macro-physical cloud property similar to the precipitation initiation height. It represents a whole cloud or even a cloud domain where aerosol and thermodynamic features do not vary considerably. Therefore it cannot be based on an individual measurement at the cloud droplet probe spatial resolution (typically ∼ 100 m), such as the maximum droplet concentration. This is because a single measurement may have a large uncertainty, be sensitive to processes on a scale too small to represent the entire cloud (e.g. local strong updraft near cloud base) and be affected by the extent of dilution that the measured cloud volume had experienced. Instead, basing the estimation of N_a on many measurements throughout the cloud and at different levels, and using a more robust micro-physical property such as R_e or R_v, is expected to be more representative and less prone to the uncertainties of the individual measurements. This is the approach we use here.

The methodology we use to derive N_a is first stated here briefly as a process that would be easy to follow. This list is followed by a more detailed description of each step with further explanations and examples from different cases for clarification.

1. Assume extreme inhomogeneous mixing. Derive a first estimation for N_a ($N_{a_{init}}$) from the slope of LWC_a to R_v^3 (or R_e^3) for AF larger than e.g. 0.25 (Fig. 2 and Eq. 1)

2. Use $N_{a_{init}}$ to calculate the relative humidity that the entrained air would have had if it was homogeneously mixed into the cloud (henceforth RH_{best}) for each horizontal cloud penetration. Figure 3a shows an example of how the results typically look.

3. Use the mean RH_{best}, derived in step 2, to estimate R_{v_a} for each penetration. Then use Eq. (1) to derive a corrected and somewhat smaller N_a (Fig. 4).

ACPD
11, 9673–9703, 2011

4. Calculate RH_{best} for each penetration again, this time based on the corrected N_a from step 3, similar to what is done in step 2 (Fig. 3). Then calculate the mean penetration residual (MPR).

5. Slightly reduce the last derived N_a (e.g. by 5%) and repeat steps 4 and 5 until MPR reaches its minimum (see example in Fig. 3b). The number of iterations for each dataset depends on the amount of N_a reduction chosen for this step.

3.1 Step 1: Calculating $N_{a_{init}}$ by assuming extreme inhomogeneous mixing

The liquid water content of a cloud parcel is the sum of masses of all droplets or the product of the droplet number concentration and the mass of a droplet with an average volume, i.e droplet whose radius is R_v. Since all small cloud droplets are spherical and the density of water is nearly constant at $1\,g\,cm^{-3}$, the number of activated CCN can be derived from the simple relationship of Eq. (1), where 10^6 is the factor so units will be [mg^{-1}], [μm] and [$g\,kg^{-1}$] for N_a, R_v and LWC_a, respectively [1].

$$N_a = 10^6 \cdot \frac{3}{4\pi} \cdot \frac{LWC_a}{R_{v_a}^3} = 62.03^3 \cdot \frac{LWC_a}{R_{v_a}^3} \quad (1)$$

R_v can be replaced by R_e by using Eq. (2) or (3) to define the parameter α for each data point [2] N is the droplet number concentration:

$$\alpha = R_e \cdot \left(\frac{N}{LWC}\right)^{\frac{1}{3}} \quad (2)$$

[1] Because we deal with rising air and change of altitude, all concentration units are per unit mass instead of the more standard volume units. We use mg^{-1} and kg^{-1} to replace cm^{-3} and m^{-3} respectively, by multiplying by the air density.

[2] Sometimes the parameter k is used instead of α for relating R_e and R_v (e.g. Martin et al., 1994). k and α are related by: $k = (\frac{62.03}{\alpha})^3$.

ACPD
11, 9673–9703, 2011

$$\alpha = 62.03 \cdot \frac{R_e}{R_v} \quad (3)$$

Typically R_e is larger by ~10% than R_v, depending on the specific shape of the droplet size spectra. Equations (2) and (3) apply for all adiabatic fractions, but a mean α should be used in order to calculate N_a, if R_{e_a} is to be used instead of R_{v_a} in Eq. (1):

$$N_a = \overline{\alpha}^3 \cdot \frac{LWC_a}{R_{e_a}^3} \quad (4)$$

The profile of LWC_a is determined by the cloud base pressure and temperature and it indicates the amount of water vapor that turned into cloud water. N_a can represent the number of activated CCN for the entire profile as long as there is no significant droplet coalescence, as it reduces the number concentration. Because the vast majority of measurements inside a deep convective cloud do not even come near the adiabatic fraction of unity, the challenge is to get a good representation of R_{e_a} based on the measurements of R_e , as R_{e_a} strongly affects N_a Eq. (4).

Freud et al. (2008) showed that R_e is not very sensitive to the degree of mixing in deep convective clouds sampled in the Amazon basin. They concluded therefore that mixing tends towards the inhomogeneous extreme. If this is the case then R_e anywhere in the cloud is expected to be close to R_{e_a}, regardless the history of the entrainment and mixing processes in the cloud. Therefore, as a first approximation, we can assume inhomogeneous mixing by using R_e instead of R_{e_a} in Eq. (4). Then N_a can be derived from the linear best fit, when plotting $R_{e_a}^3$ vs. LWC_a and calculating the mean α based on the individual data points, as shown in Fig. 2

The relationships between R_e^3 to LWC_a for different adiabatic fraction thresholds, from flight 20100226 over northern Israel, are presented in Fig. 2. The slope of each group of data points is used to calculate N_a, which we will henceforth refer to as $N_{a_{init}}$ to point out that this is the first and initial N_a estimation based on the assumption of extreme inhomogeneous mixing. One can see that only few data points have AF > 0.5

ACPD
11, 9673–9703, 2011

(the cyan data points), which means that most parts of the cloud are far from adiabatic. There is still a fairly wide range of adiabatic fractions which represents the varying proportions of cloudy and ambient air mixtures. Using filters for the different adiabatic fractions, as is represented by the different colors in Fig. 2, yields slightly smaller values of the derived $N_{a_{init}}$ for the higher adiabatic fraction thresholds. If mixing was indeed extremely inhomogeneous, $N_{a_{init}}$ would not have been dependent on AF whatsoever. However this is clearly not the case and we do see a small decrease in R_e at the smaller adiabatic fractions, which seemingly affects the derived $N_{a_{init}}$ to some extent. Because we do not have adiabatic samples throughout the vertical profile and we do not know the actual N_a, the adiabatic slope in Fig. 2 is not known. We can though still expect N_a to be slightly lower than 494 mg^{-1}, which is the $N_{a_{init}}$ calculated for AF > 0.5 in the presented case. Another added value of using AF as a filter is for excluding data points from adjacent clouds with higher bases that occasionally exist and can not always be evaded when collecting data. These clouds would have a smaller R_e in relation to the convective clouds of our interest at the same altitude, so we desire to exclude them from our analysis. The trade off of using a too high AF threshold may be that too many data points will be filtered and that the remaining data points may be concentrated at the lower part of the profile, so the derived N_a would be too sensitive to small errors in R_e and LWC_a. A good compromise would be using AF > 0.25 as the threshold for calculating $N_{a_{init}}$, which is represented by the blue data points and slope in Fig. 2. It is important to mention though that the final derivation of N_a is not sensitive to the AF threshold chosen here.

In theory and as shown in Eqs. (1) and (4), N_a is sensitive to LWC_a, therefore it is very important to document the cloud base properties (altitude, pressure and temperature) correctly. In fact, Fig. 2 may be useful in case these parameters cannot be documented because of e.g. air traffic control limitations or high terrain. This is done by prescribing different cloud base properties so that the LWC_a profile changes until the linear R_e^3 to LWC_a fit crosses the axes origin. Another incentive for deriving accurate values for LWC_a, would be the ability to use it as an envelope for the maximum cloud droplet

ACPD
11, 9673–9703, 2011

spectra integrated LWC to test the data quality of the cloud droplet probe, as integrated LWC exceeding LWC_a values may indicate an overestimation of droplet concentration and/or oversizing of the droplets. Such cases would require correction of the dataset as they affect the derived N_a.

3.2 Step 2: Using $N_{a_{init}}$ to calculate RH_{best}

$N_{a_{init}}$ derivation is based on the assumption of extreme inhomogeneous mixing. In order to improve the first estimation of N_a, the degree of actual mixing inhomogeneity must be taken into account. This can be done by examining the dependence of R_v on AF (as shown in Fig. 1), but for each horizontal penetration independently, as the degree of mixing inhomogeneity may vary with altitude because droplets grow and turbulence changes. A theoretical relative humidity that best fits each penetration data, RH_{best}, can be found by assuming homogeneous mixing and using the R_v to AF relationship as well as the values of LWC_a and $N_{a_{init}}$. RH_{best} represents the theoretical RH of the entrained air if it were homogeneously mixed with an adiabatic cloud at a specific level. The closer RH_{best} is to the real ambient RH, the stronger the tendency of the mixing towards the homogeneous limit. Figure 3 shows examples of RH_{best} fits calculated for horizontal penetrations at varying altitudes as represented by the different colors, for data collected during CAIPEEX-1 flight 20090825 over cantral India. Focusing on the left panel (Fig. 3a); the RH_{best} calculation in this panel uses $N_{a_{init}}$ as input, which determines R_{v_a} for each penetration or level. From the legend in this panel it can be seen that the mean RH_{best} is smaller than 100%, which would have been the mean in case of extreme inhomogeneous mixing for which R_v is independent on AF.

3.3 Step 3: Estimating R_{v_a} and correcting $N_{a_{init}}$

RH_{best} values smaller than 100% as were derived in the previous step, indicate that mixing is not extremely inhomogeneous. These values can be utilized to construct a new plot to improve the estimation of N_a, in a quite similar way to what is shown in

ACPD
11, 9673–9703, 2011

Fig. 2, but here without assuming extreme inhomogeneous mixing. An example for a different case is given in Fig. 4, where the blue circles show the data points with AF > 0.25 that were used to derive $N_{a_{init}}$ for that case. Here we use R_v instead of R_e to demonstrate the interchangeability of the two. Using the mean RH_{best} from the previous step enables the extrapolation of each R_v at its actual adiabatic fraction to its adiabatic value, R_{v_a}, which are shown as the red circles in Fig. 4. The new values of R_{v_a} are not based on the extreme inhomogeneous assumption, which is known to be not entirely valid, and therefore are expected to represent the real R_{v_a}, better than just assuming $R_v = R_{v_a}$. A first correction for $N_{a_{init}}$ can be made from the LWC_a to the new $R_{v_a}^3$ ratio (the slope of the linear best fit red line in Fig. 4) and Eq. (1). It is considered an improvement because instead of assuming extreme inhomogeneous mixing, homogeneous mixing with pre-moistened entrained air (with $RH = RH_{best}$) is used, which appears to be a better representation of reality (Burnet and Brenguier, 2007). This is still not the final and best estimation of N_a, because RH_{best} is based on $N_{a_{init}}$, which is known a-priori to be an overestimation of the real N_a.

3.4 Steps 4–5: Iterations for finding minimal residuals

Because RH_{best} and the estimated N_a depend on each other, N_a derived in step 3 is not necessarily the final one. In order to quantify the quality of the RH_{best} fits, which were derived by prescribing N_a, the mean penetration residual (henceforth MPR) can be calculated for the entire profile. This is done by averaging the distance of all data points from the best fit curve in each penetration separately, and then averaging all penetrations, so they get the same weight in the averaging regardless of the length of the cloud pass. The lower the MPR the better the overall RH_{best} fits.

The aim of the iterations part is to find the N_a for which MPR is minimal. Steps 1–3 brought N_a to a good starting point for the iterations, which can be considered as fine tuning of N_a. N_a should be tuned downwards, as assuming extreme inhomogeneous mixing and hence small R_{v_a}, results in higher N_a (Eq. 1) than without assuming this.

ACPD
11, 9673–9703, 2011

A reasonable step for each iteration would be to lower N_a by increments of e.g. 5%, depending on how much we trust the cloud droplet measurements themselves. MPR for each N_a iteration should be derived, based on the recalculated RH_{best} values, until the minimal MPR is found. Smaller increments will result in more iterations. The corresponding N_a is the N_a that best fits the entire profile data. This way all penetrations are equally weighted, but this still allows the degree of mixing inhomogeneity to vary with altitude and by penetration. The RH_{best} values for penetrations at different cloud depths has an added value because it can be used to assess the change in the effects of the nature of the entrainment and mixing with altitude, which has rarely been done in the past. But in order to do that there is a need for reliable and accurate profiles of RH outside the clouds, which we currently do not possess.

3.5 Remarks

It is important to point out that the final derived N_a does not depend on $N_{a_{init}}$, so using a minimum AF for deriving $N_{a_{init}}$ (in Fig. 2) other than 0.25, will only have an effect on the number of iterations needed before reaching the optimal N_a. Using a too small minimum AF and including data from clouds with higher bases, may result in a mean RH_{best} of 100%, which will not allow the first correction of $N_{a_{init}}$ (step 3). On the other hand, using a too high AF filter may lead to a too low and unreliable $N_{a_{init}}$ value in case it is based on too few data points from the lower part of the cloud, which could be smaller than the actual N_a. Therefore it is advisable to plot the data as shown in Fig. 2 and choose a proper minimum AF to base $N_{a_{init}}$ on.

Moreover, it should also be mentioned that the method described here is valid as long as the droplet number concentration per unit mass of air in an adiabatic parcel remains constant, i.e. droplets grow mainly by condensation with little coalescence that leads to reduction of droplet concentration, and there is no nucleation of new cloud droplets that would increase it. Nucleation of new droplets by entrained CCN (or those that were not activated near cloud base) can occur in case there is a combination of low droplet concentration and accelerating updrafts. In real clouds it is more likely to occur

ACPD
11, 9673–9703, 2011

in highly diluted parts of the clouds, so defining a threshold AF as filter can be useful to exclude these cases, as well as those cases with data contamination by clouds with higher bases than the clouds of our interest. In addition, droplet concentration is lowered when droplet coalescence is significant and during rainout, so the data set should be based upon young growing convective clouds before the droplets have the chance to grow large enough for significant coalescence. Normally this occurs when R_e reaches ~12 µm (Freud and Rosenfeld, 2011).

4 Results and discussion

We applied the methodology described in the previous section to data collected in deep convective clouds over Israel, India, the Amazon, Texas and California, under a variety of meteorological conditions and aerosol characteristics. N_a was derived for each cloud profile (the profiling was not Lagrangian, but rather penetrating tops of consecutively growing convective clouds in a cloud cluster) and it ranged between 100 to 2500 per milligram of air, which occupies a volume of approximately 1 cm^3 at a typical cloud base altitude of 1.5 km a.s.l.

Adding an error bar to the derived N_a at the end of the routine described in Sect. 3 is not an easy task. This is because it mainly depends on the calibration and performance of the specific cloud droplet probe. An advantage is that the routine relies more on the sizing accuracy of the probe rather than on the concentration measurements. Testing the sizing calibration by releasing glass beads across the probe laser beam is something that is normally done quite often during a field campaign. Our experience shows that drift in the concentration calibration is more common, therefore it is important to correct this drift in the data analysis phase by e.g. comparing the cloud droplet probe integrated LWC with the Hot Wire LWC, which is usually more reliable as the measurement is quite straight forward in comparison with the cloud droplet probe. Then the droplet concentration could be multiplied by the calculated correction factor, which may change even during flight, while leaving the shape of the droplet size

ACPD
11, 9673–9703, 2011

distribution unchanged. Another key point for minimizing uncertainty in N_a estimation, is to avoid mixing clouds with bases at different altitudes or with varying aerosol or thermodynamic properties in the same analysis. Such cases would cause a fairly large variation in R_e for a given LWC_a, which is calculated for the lowermost cloud base. In order to exclude data from penetrations to clouds with elevated bases, a filter based on a minimum adiabatic fraction can be used (like in the example shown in Fig. 2). Furthermore, penetrations with well developed warm rain or ice formation should also be excluded from the analysis as large fraction of the drops are lost to hydrometeors and the spectra of the remaining drops are altered, hence changing R_e, R_v and AF. If these requirements are satisfied, and the steps described in Sect. 3 are followed, the derived N_a is expected to represent quite well the number of activated CCN in a cloud or field of microphysically similar clouds.

At the end of Sect. 2 we mentioned that the RH of the ambient air together with what we defined in Sect. 3 as RH_{best}, can be used to assess the degree of mixing inhomogeneity. Unfortunately we do not have accurate and reliable RH data, but analyzing the derived RH_{best} values for many penetrations can still be informative. Figure 5 shows the derived RH_{best} values of more than 500 penetrations in convective clouds over Israel, India, the Amazon and Texas, versus the adiabatic water mixing ratio for each penetration, which is a representation of the vertical dimension. There is of course a fair amount of scatter in the data, but the median RH_{best} is 95.25%. This value is definitely higher than the typical RH aloft between the convective clouds, and therefore an indication that in the vast majority of cases, the entrainment-mixing process is far from homogeneous. A closer look on RH_{best} in the vertical dimension may give the impression that there is a weak tendency towards smaller RH_{best} values at larger cloud depths or at least that the highest RH_{best} occurences are concentrated near cloud base. This may be interpreted as a weak tendency towards homogeneous mixing at greater altitudes, as Small and Chuang (2010) reported in their study based on few cases, but by using slightly different methods. A possible explanation for this trend is that turbulence aloft is more pronounced due to stronger updrafts aloft, so τ_{mix} is decreased. In

ACPD
11, 9673–9703, 2011

addition the droplets are larger aloft so τ_{evap} is increased for a given RH. This results in a decrease in the Damköhler ratio and hence a tendency towards homogeneous mixing aloft. Since we do not have accurate profiles of ambient RH in the cloud-free air, our dataset does not enable us to rule out that all apparent RH_{best} decrease aloft can be explained by a decrease of ambient RH with altitude, which is not uncommon in an unstable atmosphere with convective clouds. In addition, in the simple model results shown in Fig. 1, as in earlier publications, the mixing of entrained air is assumed to occur with an adiabatic parcel at a constant level. This is of course not necessarily true, as different parcels in the clouds may have been exposed earlier to entrained air at other altitudes. In convective clouds, the air can move vertically quite rapidly, so if a mixing event at a low altitude already caused a small reduction in R_v, and another mixing event higher up caused an additional small reduction in R_v, the combined effect will result in a smaller derived RH_{best} when we assume exclusive one-level mixing. This is because we would have a higher reference value – R_{v_a}. It will be interpreted as a trend towards homogeneous mixing aloft and may partly contribute to the tendency seen in Fig. 5. So without reliable and accurate RH measurements outside the clouds, we cannot say that we found proof for clear tendency towards less inhomogeneous mixing higher in the cloud, but clearly mixing has a general tendency towards the inhomogeneous limit at all levels as indicated by the high RH_{best} values. Our interpretation of this result is that the entrained drier air quickly causes a total evaporation of the cloud droplets that border the entrained parcel, so the entrained air gets more moist but cannot be considered as a cloud at that point. As it approaches saturation, the molecular diffusion of vapor from the droplets to the sub-saturated air slows down, increasing the time scale of the droplet evaporation, so further turbulent mixing with the cloud tends to be more homogeneous. It appears that the entrained air is pre-moistened (this term has been used by Burnet and Brenguier, 2007) in a nearly extreme inhomogeneous manner and then is mixed more homogeneously as it approaches saturation. Small and Chuang (2010) compared edges and cores of clouds and found a similar tendency.

ACPD
11, 9673–9703, 2011

As discussed in Sect. 3, taking into account the mixing inhomogeneity is important for obtaining a better estimation for N_a. The example in Fig. 3 shows that using the final N_a (panel b), as compared to $N_{a_{init}}$ (panel a) that is based on the extreme inhomogeneous mixing assumption, results in improved overall fits of the RH_{best} curves to the data points. This example is not unique, we find similar improvements in all analyzed profiles. The difference between N_a and $N_{a_{init}}$ is on average ~30%, as Fig. 6 shows, regardless of location. This means that it is important to account for the relative inhomogeneity of the mixing at all levels despite the high median RH_{best} (95.25%), which clearly indicates a strong tendency towards the extreme inhomogeneous mixing limit. What is also evident in Fig. 6 is that all data points fall above the 1:1 dashed line. This is because the inhomogeneous mixing assumption, which is used to derive $N_{a_{init}}$, marks the upper limit of the N_a estimation. If the actual mixing is more inhomogeneous, then the difference between N_a and $N_{a_{init}}$ will be less pronounced.

N_a, being an estimation of the number of activated CCN, can be compared against the CCN concentrations at a given super-saturation that were measured below cloud base. This may reveal some information about the CCN activation process and/or instrument performance. Such a comparison is shown Fig. 7. This plot displays data from different locations, instruments and super-saturations, as indicated in the figure legend. A perfect fit between the CCN concentration at a given super-saturation and N_a should not be expected because N_a encapsulates the information about cloud base updraft, which the CCN concentration is independent of. Despite that, the linear fit for each location separately, shown in Fig. 7, is fairly good ($R > 0.87$), but the different locations exhibit significantly different slopes. This is probably due to the different instrumentation and calibrations used in each location and optionally different cloud base updrafts. Taking into account the common cloud base updraft speed may help explain some of the differences between the locations. However the relatively small variability of the fit within a location indicates that the variability in updrafts cannot explain the very different fits. This would be mainly caused by the cloud drop spectrometer sizing and counting errors, as well as the different calibrations of the CCN counters. If the cloud

ACPD
11, 9673–9703, 2011

droplet probe is calibrated properly and performs well, the N_a to CCN relationship can be used to roughly estimate the average cloud base updraft, providing that the CCN spectra is known. That would be one example of an applicable use of N_a.

5 Summary and conclusions

The study presented here aims at deriving the number of activated CCN into cloud droplets in deep convective clouds that are prone to significant mixing with entrained dry air, due to their relatively small horizontal extent, strong turbulence and the fact that they tend to grow into sub-saturated layers of air. Here we present a methodology for deriving N_a from data of substantially sub-adiabatic clouds, by first assuming that the entrainment and mixing of air into the cloud is extremely inhomogeneous. This yields the upper limit for N_a, which we refer to as $N_{a_{init}}$ and that serves as a starting point for the fine tuning of the final N_a derivation as well as to obtain information regarding the nature of the mixing process between the cloudy and the entrained sub-saturated ambient air.

The N_a derivation methodology regards the cloud, or set of clouds, as a unity, so N_a is more like a macro-physical property of the cloud or the cloudy domain, as long as aerosol properties and thermodynamics are fairly homogeneous. N_a represents the typical number concentration of CCN that are activated into cloud droplets in the updrafts at the cloud base. It is initially based on the entire profile data and then tuned based on data of individual cloud penetrations. In order to apply this methodology it is necessary to penetrate convective clouds at different levels. Preferably in horizontal penetrations from cloud base to the level where significant precipitation is formed (i.e. not precipitation falling from above). Significant precipitation for that matter means that more than about 5% of the cloud water has been converted into hydro-meteors. The described methodology may also be applied to shallow convective clouds, but the confidence in the derived number may be reduced due to the smaller span of droplet

ACPD
11, 9673–9703, 2011

sizes and higher sensitivity to the correctness of the cloud base properties input data and greater sensitivity to uncertainty in cloud droplet probe measurements. Applying the methodology to stratiform clouds is typically not as advantageous compared to the methods that have been used already for such clouds (e.g. Bennartz, 2007) because nearly adiabatic cloud parcels, in which droplet concentrations are essentially N_a, are very common.

After applying the methodology described in Sect. 3 to a large set of data collected in Israel, India, the Amazon, Northwestern Europe, Texas and California, we conclude the following:

- R_v^3 (and R_e^3) grows nearly linearly with the adiabatic water mixing ratio in deep convective clouds before significant droplet coalescence takes place, at a rate that primarily depends on N_a.
- N_a is closely related to the CCN concentrations. Typical updrafts and cloud base super-saturations may be derived from this relationship and the measured CCN activation spectra.
- Mixing of sub-saturated air into the cloud is strongly inhomogeneous, but does not reach the extreme inhomogeneous limit. It appears like the entrained air is pre-moistened by quickly evaporating cloud droplets initially and then mixes more homogeneously as it approaches saturation.
- It appears like mixing is less inhomogeneous higher in the cloud due to the larger cloud droplets and stronger turbulence there. Drier air aloft and the history of mixing at lower levels of the cloud may also contribute the this observed trend.

Acknowledgements. This study is part of the Ph.D thesis of Eyal Freud at the Hebrew University of Jerusalem, with Daniel Rosenfeld as his Ph.D adviser. Some of the examples rely in parts on data obtained from the Cloud Aerosol Interaction and Precipitation Enhancement Experiment (CAIPEEX) of the Indian Institute of Tropical Meteorology (IITM), with J. R. Kulkarni

ACPD
11, 9673–9703, 2011

as a program manager and B. N. Goswami as the director. Additional examples are based on data from Texas, with D. Axisa having taken the lead on the instrumented aircraft, data collection and quality control. Some additional aircraft data are taken from the European Integrated Project on Aerosol Cloud Climate Air Quality Interactions (EUCAARI) in northwestern Europe, and from the Smoke Aerosols, Clouds, Rainfall and Climate (SMOCC) aircraft campaign in the Amazon. Both EUCAARI and SMOCC were funded by the European Commission. Data are used also from the research flights of the Israeli rain enhancement program funded by the Israeli Water Authority, and from the SUPRECIP campaign in California, funded by the California Energy Commission. The authors would like to express their gratitude to all sponsors, partners and collaborators for their efforts in collecting these valuable and extensive datasets.

References

Albrecht, B. A.: Aerosols, Cloud Microphysics and Fractional Cloudines, Science, 245, 1227–1230, 1989. 9675

Andreae, M. O.: Correlation between cloud condensation nuclei concentration and aerosol optical thickness in remote and polluted regions, Atmos. Chem. Phys., 9, 543–556, doi:10.5194/acp-9-543-2009, 2009. 9676

Andreae, M., Rosenfeld, D., Artaxo, P., Costa, A., Frank, G., Longo, K., and Silva-Dias, M.: Smoking rain clouds over the Amazon, Science, 303, 1337, doi:10.1126/science.1092779, 2004. 9701

Axisa, D., Rosenfeld, D., Santrpia, J., Woodley, W., and Collins, D.: The Southern Plains Experiment in Cloud Seeding of Thunderstorms for Rainfall Augmentation (SPECTRA) Project: Operational tools used towards 470 verifying glaciogenic and hygroscopic seeding conceptual models, case studies and preliminary results, in: 16th Conference on Planned and Inadvertent Weather Modification, 2005. 9701

Baker, M. B., Corbin, R. G., and Latham, J.: The Influence of entrainment on the evolution of cloud droplet spectra. 1. A model of inhomogeneous mixing, Q. J. Roy. Meteor. Soc., 106, 581–598, 1980. 9678

Baker, M. B., Breidenthal, R. E., Choularton, T. W., and Latham, J.: The Effects of Turbulent Mixing in Clouds, J. Atmos. Sci., 41, 299–304, 1984. 9677

Bennartz, R.: Global assessment of marine boundary layer cloud droplet number concentration

ACPD
11, 9673–9703, 2011

from satellite, J. Geophys. Res.-Atmos., 112, D02201, doi:10.1029/2006JD007547, 2007. 9676, 9692
Blyth, A. M., Choularton, T. W., Fullarton, G., Latham, J., Mill, C. S., Smith, M. H., and Stromberg, I. M.: The Influence of entrainment on the evolution of cloud droplet spectra. 2. Field experiments at Great Dun Fell, Q. J. Roy. Meteor. Soc., 106, 821–840, 1980. 9678
Bower, K. and Choularton, T.: The effects of entrainment on the growth of droplets in continental cumulus clouds, Q. J. Roy. Meteor. Soc., 114, 1411–1434, 1988. 9679
Brenguier, J. L.: Observations of Cloud Microstructure at the Centimeter Scale, J. Appl. Meteorol., 32, 783–793, 1993. 9677
Brenguier, J. L., Pawlowska, H., Schuller, L., Preusker, R., Fischer, J., and Fouquart, Y.: Radiative properties of boundary layer clouds: Droplet effective radius versus number concentration, J. Atmos. Sci., 57, 803–821, 2000. 9676
Burnet, F. and Brenguier, J. L.: Observational study of the entrainment-mixing process in warm convective clouds, J. Atmos. Sci., 64, 1995–2011, 2007. 9679, 9685, 9689
Dimotakis, P. E.: Turbulent mixing, Ann. Rev. Fluid Mech., 37, 329–356, 2005. 9678
Freud, E. and Rosenfeld, D.: A new look into the relation between cloud drop number concentration and depth for rain initiation in deep convective clouds, in: 91st American Meteorological Society Annual Meeting, American Meteorological Society, Seattle, WA, 2011. 9687
Freud, E., Rosenfeld, D., Andreae, M. O., Costa, A. A., and Artaxo, P.: Robust relations between CCN and the vertical evolution of cloud drop size distribution in deep convective clouds, Atmos. Chem. Phys., 8, 1661–1675, doi:10.5194/acp-8-1661-2008, 2008. 9679, 9682
Gerber, H.: Entrainment, mixing, and microphysics in RICO cumulus, in: Proc. 12th Conf. On Cloud Physics, 2006. 9679
Hill, T. and Choularton, T.: An airborne study of the microphysical structure of cumulus clouds, Q. J. Roy. Meteor. Soc., 111, 517–544, 1985. 9679
IPCC: Climate Change 2007 – The Physical Science Basis. Contribution of Working Group 1 to the Fourth Assessment Report of the Intergovernmental Panel on Climate Change, Cambridge University Press, Cambridge, UK and New York, 2007. 9675
Jensen, J. and Baker, M.: A Simple Model of Droplet Spectral Evolution during Turbulent Mixing, J. Atmos. Sci., 46, 2812–2829, 1989. 9679
Koren, I., Remer, L. A., Altaratz, O., Martins, J. V., and Davidi, A.: Aerosol-induced changes of convective cloud anvils produce strong climate warming, Atmos. Chem. Phys., 10, 5001–5010, doi:10.5194/acp-10-5001-2010, 2010. 9675

ACPD
11, 9673–9703, 2011

Kulkarni, J., Maheskumar, R., Konwar, M., Deshpande, C., Morwal, S., Padma Kumari, B., Joshi, R., Pandithurai, G., Bhalwankar, R., Mujumdar, V., Goswami, B., and Rosenfeld, D.: The Cloud Aerosol Interactions and Precipitation Enhancement Experiment (CAIPEEX): overview and prominent results, in: AGU Fall Meeting Abstracts, 1, p. 01, 2009. 9699

Kulmala, M., Asmi, A., Lappalainen, H. K., Carslaw, K. S., Pöschl, U., Baltensperger, U., Hov, Ø., Brenquier, J.-L., Pandis, S. N., Facchini, M. C., Hansson, H.-C., Wiedensohler, A., and O'Dowd, C. D.: Introduction: European Integrated Project on Aerosol Cloud Climate and Air Quality interactions (EUCAARI) - integrating aerosol research from nano to global scales, Atmos. Chem. Phys., 9, 2825–2841, doi:10.5194/acp-9-2825-2009, 2009. 9702

Latham, J. and Reed, R. L.: Laboratory studies of effects of mixing on evolution of cloud droplet spectra, Q. J. Roy. Meteor. Soc., 103, 297–306, 1977. 9678

Lehmann, K., Siebert, H., and Shaw, R. A.: Homogeneous and Inhomogeneous Mixing in Cumulus Clouds: Dependence on Local Turbulence Structure, J. Atmos. Sci., 66, 3641–3659, 2009. 9677, 9678

Martin, G., Johnson, D., and Spice, A.: The Measurement and Parameterization of Effective Radius of Droplets in Warm Stratocumulus Clouds, J. Atmos. Sci., 51, 1823–1842, 1994. 9681

Paluch, I.: Mixing and the Cloud Droplet Size Spectrum: Generalizations from the CCOPE Data, J. Atmos. Sci., 43, 1984–1993, 1986. 9679

Paluch, I. and Baumgardner, D.: Entrainment and fine-scale mixing in a continental convective cloud, J. Atmos. Sci., 46, 261–278, 1989. 9679

Pawlowska, H., Brenguier, J. L., and Burnet, F.: Microphysical properties of stratocumulus clouds, Atmos. Res., 55, 15–33, 2000. 9677, 9679

Rosenfeld, D., Lohmann, U., Raga, G. B., O'Dowd, C. D., Kulmala, M., Fuzzi, S., Reissell, A., and Andreae, M. O.: Flood or drought: How do aerosols affect precipitation?, Science, 321, 1309–1313, 2008a. 9675

Rosenfeld, D., Woodley, W., Axisa, D., Freud, E., Hudson, J., and Givati, A.: Aircraft measurements of the impacts of pollution aerosols on clouds and precipitation over the Sierra Nevada, J. Geophys. Res, 113, D1503, doi:10.1029/2007JD009544, 2008b. 9702

Schüller, L., Brenguier, J. L., and Pawlowska, H.: Retrieval of microphysical, geometrical, and radiative properties of marine stratocumulus from remote sensing, J. Geophys. Res.-Atmos., 108, 8631, doi:10.1029/2002JD002680, 2003. 9676

Small, J. D. and Chuang, P. Y.: An analysis of entrainment mixing processes in warm cumu-

ACPD
11, 9673–9703, 2011

lus, in: 13th Conference on Cloud Physics, American Meteorological Society, Portland, OR, 2010. 9688, 9689
Snider, J. R., Leon, D., and Wang, Z.: Cloud droplet number concentration in VOCALS-REx, in: 13th Conference on Cloud Physics, American Meteorological Society, Portland, OR, 2010. 9676
Twomey, S.: Pollution and Planetary Albedo, Atmos. Environ., 8, 1251–1256, 1974. 9675, 9676

ACPD
11, 9673–9703, 2011

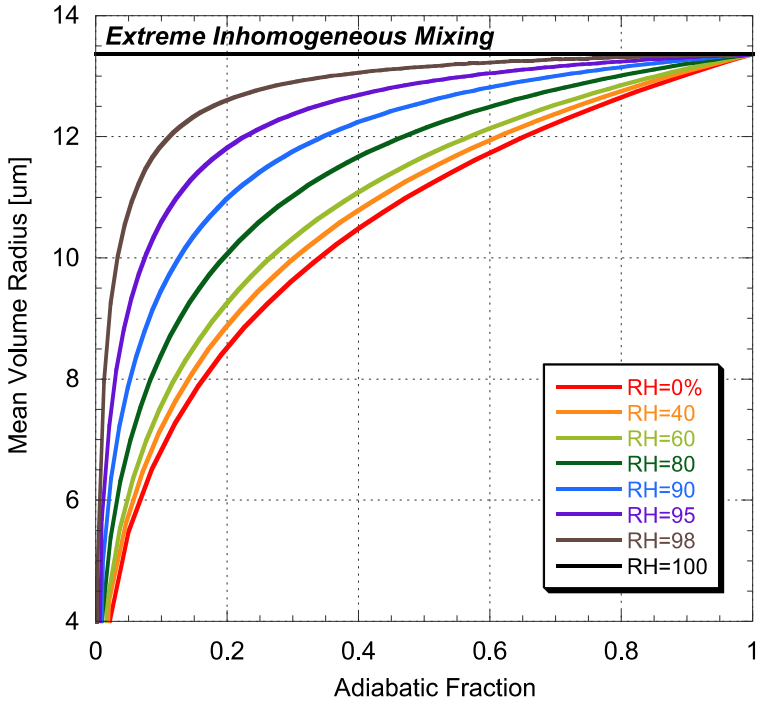

Fig. 1. Mixing diagram: the relationship between droplet mean volume radius (R_v) and the adiabatic fraction (AF) for fully homogeneous and extreme inhomogeneous mixing events between an adiabatic cloud parcel and entrained non-cloudy air with varying relative humidity (RH) at the mixing level of ~2200 m above cloud base, where the temperature is ~10 °C and the adiabatic mixing ratio is 5 g kg^{-1}. Cloud base is at 850 hPa and 20 °C. Concentration of activated CCN (N_a) is 500 mg^{-1}. It can be seen that entrained air with higher RH results in smaller dependence of R_v on AF, especially for AF > 0.2. When entrained air is saturated (RH = 100%), or when mixing is extremely inhomogeneous, R_v is constant.

ACPD
11, 9673–9703, 2011

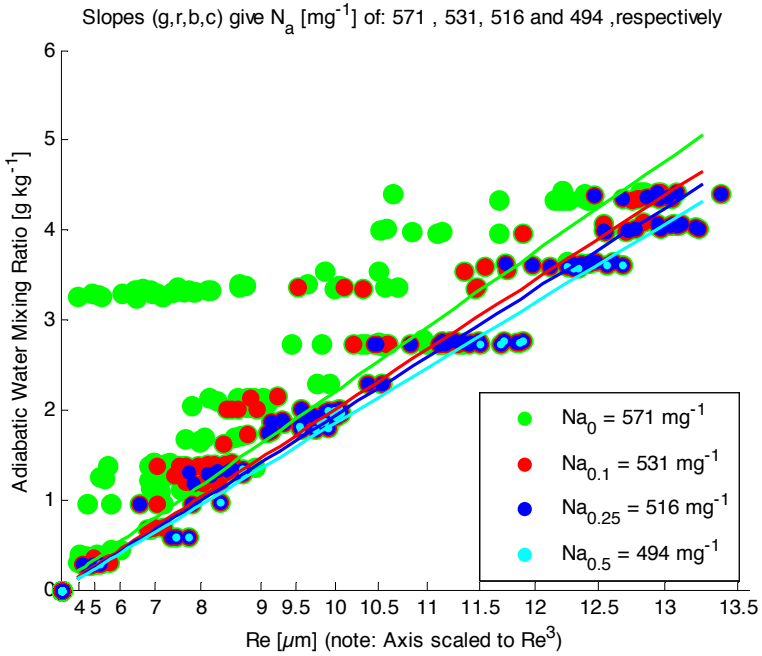

Fig. 2. Cloud droplet effective radius vs. Adiabatic Water for different threshold adiabatic fractions for flight 20100226 over Israel. Green, red, blue and cyan for minimum adiabatic fractions of 0, 0.1, 0.25 and 0.5, respectively. R_e and AF data are based on the Droplet Measurement Technologies (DMT) Cloud Droplet Probe (CDP) measurements and the activated CCN is derived by the slope of the linear best fit (Eq. 4). It can be seen that the AF filter selected does not affect the derived N_a significantly, except for the lowermost one, which is required for excluding data of very diluted clouds and clouds with elevated bases that have small R_e but fairly high adiabatic water if the main cloud base parameters are used. Using $N_{a_{0.25}}$ as $N_{a_{init}}$ looks like a reasonable compromise between having enough data points to represent the entire profile, and having a large LWC_a range for deriving a representative $N_{a_{init}}$ for the entire profile.

ACPD
11, 9673–9703, 2011

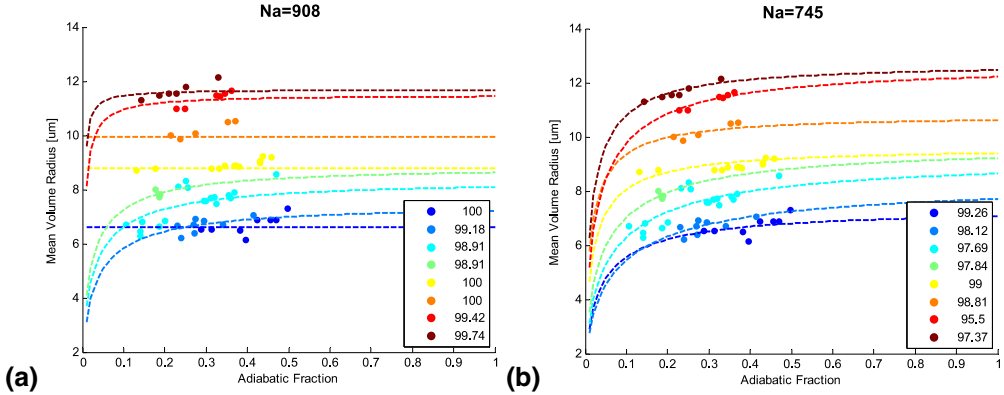

Fig. 3. (a) RH_{best} fits (see text for description) for horizontal cloud penetrations, represented by different colors. Each data point is based on the CDP 1 Hz measurement. The measurements were taken during the CAIPEEX-1 (Cloud-Aerosol Interaction and Precipitation Enhancement Experiment, phase 1; Kulkarni et al., 2009) program over central India on 25 August 2009 at elevations between 500 and 5000 m. $N_{a_{init}}$ is used to calculate RH_{best} for each penetration whose derived value is shown in the legend. **(b)** Same as **(a)**, but with the final derived N_a (see Sect. 3.4) to best fit the same data. Even with the naked eye this panel shows a better overall fit than the left panel.

ACPD
11, 9673–9703, 2011

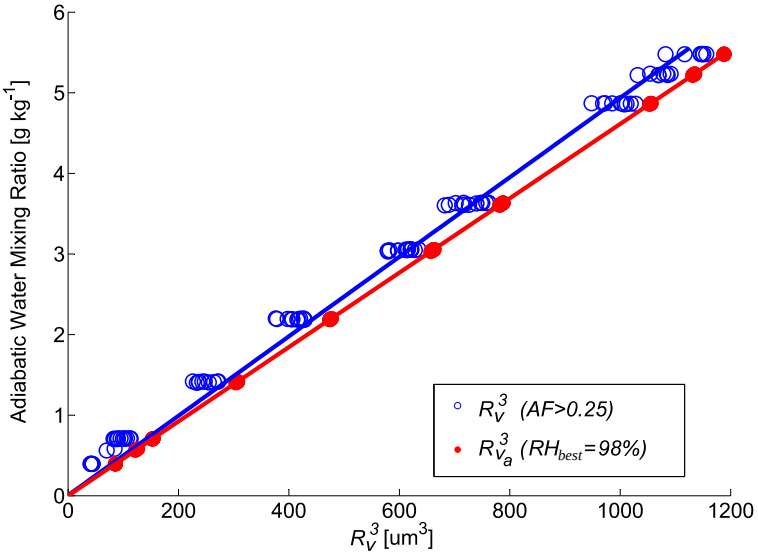

Fig. 4. R_v^3 (blue circles) and $R_{v_a}^3$ (red circles) vs. the adiabatic water mixing ratio. The blue and red linear best fits are used to derive $N_{a_{init}}$ (1101 mg^{-1}) and N_a (895 mg^{-1}), respectively. The blue circles represent all data points with AF > 0.25 from CAIPEEX-1 flight 20090814 in a deep convective cloud over central India. The red circles represent the extrapolated R_v to their adiabatic values R_{v_a}, by assuming the mean RH_{best} for all profile penetrations in order to get a more realistic N_a that is not based on the extreme inhomogeneous mixing assumption.

ACPD
11, 9673–9703, 2011

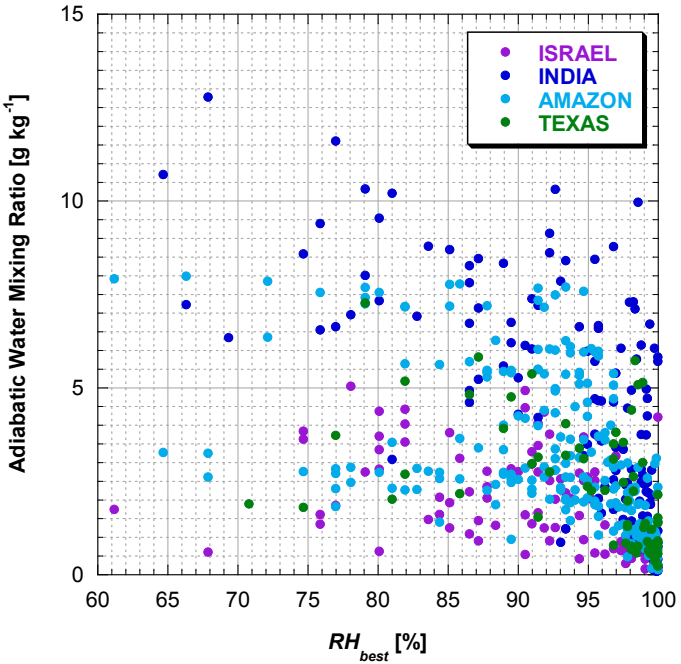

Fig. 5. The calculated RH_{best} for each penetration (based on the derived N_a of each profile) vs. LWC_a, which relates to the vertical dimension. The color-coding represents the different field campaign and location data: purple for the Israeli rain enhancement program; blue for CAIPEEX-1 in India; Cyan for the Large-Scale Biosphere-Atmosphere Experiment in Amazonia – Smoke, Aerosols, Clouds, Rainfall, and Climate (SMOCC; Andreae et al., 2001); and green for SPECTRA (The Southern Plains Experiment in Cloud seeding of Thunderstorms for Rainfall Augmentation; Axisa et al., 2005). It appears like the highest RH_{best} values are found near cloud base, indicating strong tendency towards extreme inhomogeneous mixing, maybe due to the small droplets and fairly weak turbulence there.

ACPD
11, 9673–9703, 2011

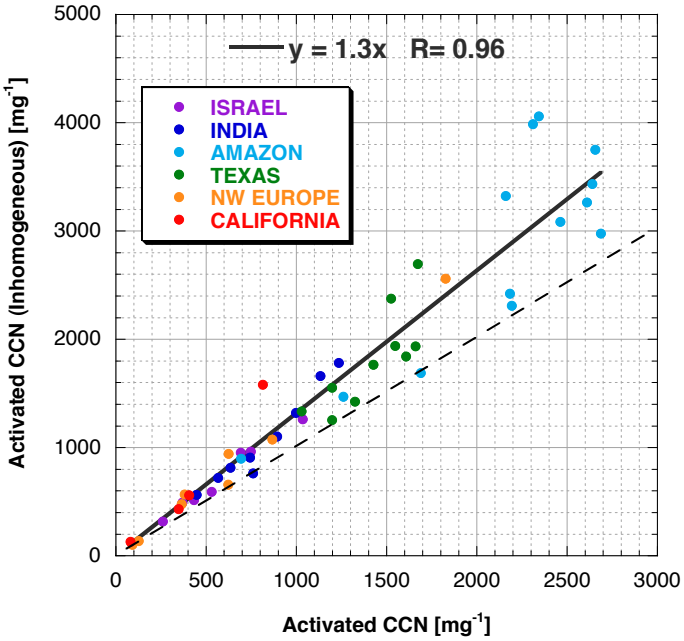

Fig. 6. Comparison of $N_{a_{init}}$, which is based on extreme inhomogeneous mixing assumption, with the final derived N_a, based on homogeneous mixing with pre-moistened air assumption. Color-coding is the same as in Fig. 5, with added data from flights within the projects of EU-CAARI (European Integrated project on Aerosol Cloud Climate and Air Quality interactions; Kulmala et al., 2009) over the Netherlands and the North Sea (in orange) and SUPRECIP (Suppression of Precipitation Experiment; Rosenfeld et al., 2008b) over California (in red). On average, N_a is smaller than $N_{a_{init}}$ by approximately 30%. It does not appear like there are significant differences between the different locations, as they fall within the same range of slopes, although the Amazon and Texas data stand out for having generally high and maybe slightly unreasonable values of N_a, which may be an indication of droplet under-sizing by the cloud droplet probes.

ACPD
11, 9673–9703, 2011

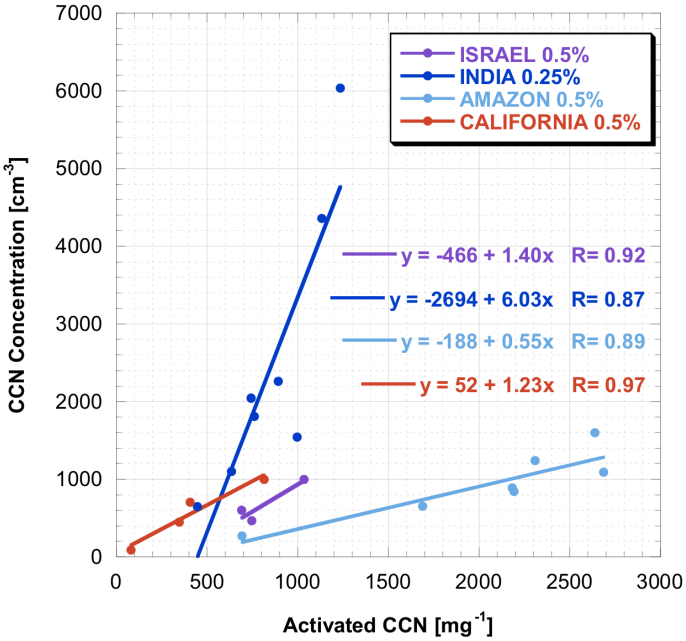

Fig. 7. The derived cloud profile N_a compared against the corresponding CCN concentrations below cloud base (measured with DMT CCN counters) at different locations and super-saturations as indicated in the legend and the captions of Figs. 5 and 6. Notice the fairly strong linear relationship for each field campaign separately. The different slopes cannot be fully explained by differing updrafts and super-saturations, but rather by the different instruments and calibrations used.

ACPD
11, 9673–9703, 2011